Sinking rates, orientation, and behavior of pennate diatoms

M Sourisseau, J Font-muñoz, S Bellouche, O Fauvarque, J Rouxel, M Tardivel, A Sauvey

Received: 2 November 2023 | Accepted: 21 March 2024

DOI: 10.1111/jpy.13463

RESEARCH ARTICLE

Sinking rates, orientation, and behavior of pennate diatoms

M. Sourisseau[1] | **J. Font-Muñoz**[1,2] | **S. Bellouche**[1] | **O. Fauvarque**[3] | **J. Rouxel**[3] | **M. Tardivel**[3] | **A. Sauvey**[4]

[1]Ifremer, DYNECO, Plouzané, France

[2]Mediterranean Institute for Advanced Studies, IMEDEA (UIB-CSIC), Esporles, Spain

[3]Ifremer, RDT Research and Technological Development, Plouzané, France

[4]Laboratoire Biologie des Organismes et Ecosystèmes Aquatiques, UMR 8067 BOREA, Normandie Université, Unicaen, Caen, France

Correspondence
M. Sourisseau, Ifremer, DYNECO, Plouzané F-29280, France.
Email: marc.sourisseau@ifremer.fr

Funding information
postdoctoral fellowship- Margalida Comas, Grant/Award Number: PD/018/2020; ISblue, Grant/Award Number: ANR-17-EURE-0015

Editor: N. Poulsen

Abstract

Phytoplankton cells are now recognized as dynamic entities rather than as passive and isolated particles because they can actively modulate impacts of selection factors (nutrients, light, turbidity, and mixing) through a wide range of adaptations. Cell shape and/or chain length modulation is one of these processes but has predominantly been studied as an adaptation or an acclimatation to a specific growth limitation (light, nutrients, predation, etc.). In this study we have demonstrated that cell shape and size may have greater roles than previously known in phytoplankton ecology and species adaptation by permitting cell-to-cell signaling and more complex ecological processes that result from it. By exploring microscale biophysical interactions that lead to specific cell reorientation processes, we demonstrated that cell geometry not only modulates cell sinking rates but can also provide fast sensor responses to the cells' environment. Although gyrotaxis has been described in detail for motile phytoplankton cells, our findings illustrate that the reorientation process described here can occur even in non-motile cells within their natural environment. An additional consistent behavior was also recently described for a diatom species (*Pseudo-nitzschia delicatessima*), and with this study, we extend this observation to *Pseudo-nitzschia pungens* and *Pseudo-nitzschia fraudulenta*. Our observations emphasize the generality of this process, which adds a new level of complexity to our understanding of cellular interactions and their network of sensors.

KEYWORDS
behavior, diatom, interaction, microscale, pennate, *Pseudo-nitzschia*, settlement

INTRODUCTION

In ocean ecosystems, particularly in tidal coastal waters, the levels of turbidity (May et al., 2003) and mixing (Carter et al., 2005) are highly variable, serving as the primary drivers of key biological rates among unicellular eukaryotes, such as the cell-encounter, sinking, and growth rates (Karp-Boss et al., 1996). Contrary to the traditional view of pelagic phytoplankton cells as passive particles (Zehr et al., 2017), it is now evident that they actively regulate their sedimentation process and encounter rates through adaptations that are widely distributed across the phytoplankton phylogeny (Wirtz & Smith, 2020). This active control likely contributes significantly to the observed diversity in their size and shape (Naselli-Flores et al., 2007; Padisák et al., 2003) as well as the success of the morphology-based functional groups approach (Kruk & Segura, 2012).

Abbreviations: FCM, flow cytometry; FWS, forward scatter; LISST, laser in-situ scattering and transmissometry; PCR, polymerase chain reaction; TEM, transmission electron microscopy.

The evolutionary trajectory of phytoplankton species has given rise to three overarching processes to regulate their vertical distribution and encounter rate. The first involves the acquisition of motility capacities, a well-described process for flagellated phytoplankton such as dinoflagellates. The second process is based on the regulation of cell buoyancy, which is achieved through a variety of morphological and physiological modifications (e.g., cell size, surface-volume ratio, lipid accumulations, gas vesicles, density regulation of vacuoles, etc.; Raven & Beardall, 2022). This process and its regulation, according to the environmental conditions, has been described for numerous phytoplankton species (Walsby, 1978), including diatoms (Eppley et al., 1967; Gemmell et al., 2016; Gross et al., 1997, Anderson & Sweeney, 1978). The last group of processes is based on cell shape and microscale biophysical interactions that lead to specific cell orientations (Visser & Jonsson, 2000) and influence encounter rates in low-Reynolds-number flows (Słomka & Stocker, 2020). For instance, assuming cells have neutral buoyancy, their elongation can modulate their encounter rates by up to one order of magnitude (Arguedas-Leiva et al., 2022) through their orientation (Li et al., 2013; Talapatra et al., 2013). Recent studies have also reported consistent behaviors of two diatom species with an oblong shape, adding new complexity to cell-to-cell interactions and their ecology (Font-Muñoz et al., 2021).

It should be also pointed out that the description of these processes is of primary importance because it involves cellular constraints and metabolic costs. These adaptations should therefore have a feedback effect on the fitness of species with regard to their environment, their spatial distribution, and their phenology over the years. Attempts to map relevant phytoplankton traits over the past decades have thus quickly identified the following as key parameters of the mobility and the sinking rates of phytoplankton cells. Margalef (1978) was one of the first researchers to divide phytoplankton into two extreme classes on a continuum of life history between *r* and *K* strategies that could be represented along a gradient of decreasing nutrient concentrations and turbulence. However, the grouping of phytoplankton species based on their traits may be biased because trait values are only available for a limited number of species (Weithoff, 2003), and traits are not always vertically conserved in the phylogeny (Kruk et al., 2010) without taking intraspecific variability into account (Brandenburg et al., 2018). Thus, it is risky to extrapolate a trait from one species to another. In this regard, few phytoplankton sinking-rate and cell-orientation measurements are available (Walsby & Holland, 2006). After the description of a new relevant behavior for *Pseudo-nitzschia delicatissima* (Font-Muñoz et al., 2021), we wanted to estimate the intra- and inter-specific variability of these two biological processes within the *Pseudo-nitzschia* genus, which contains several toxic species and creates serious management problems in coastal waters. As a result, different methodologies were used for the two additional species to accurately describe their sinking rates and cell behaviors.

METHODS

Cultures

A total of seven and 12 strains of *Pseudo-nitzschia pungens* and *P. fraudulenta,* respectively, were used (Table 1). Cultures were maintained in 80 mL of sterile-filtered oligotrophic seawater amended with nutrients (K/2) at 17°C, under a 12:12 light:dark cycle and a light intensity of 80 $\mu E \cdot m^{-2} \cdot s^{-1}$, in algal incubators. The strains were initially identified using transmission electron microscopy (TEM) and confirmed by molecular analysis. Genomic DNA was extracted using the DNeasy Plant Mini Kit (cat. no. 69104 and 69106), and polymerase chain reaction (PCR) was performed with the PN PNS-F1 primer: GGA-TCA-TTA-CCA-CAC-CGA-TCC and PSN-R1: CCT-CTT-GCT-TGA-TCT-GAG-ATC-C; Noyer et al., 2015). Cultures were diluted once a week to stay in their exponential growing phase with high cell densities ($>10^8$ particles $\cdot L^{-1}$). All of the following experiments were performed in triplicate for

TABLE 1 Location and isolation time of the cultivated strains.

Strain label	Location	Sampling date	Species
P19_1/PN_P1	Cabourg	May 2019	*P. pungens*
P19_3/PN_P2	Luc-sur-Mer	April 2019	"
P19_4/PN_P3	"	"	"
P19_5/PN_P4	"	"	"
P19_6/PN_P5	"	"	"
P19_7/PN_P6	"	"	"
P19_12/PN_P7	"	"	"
P20_1/PN_F1	"	June 2020	*P. fraudulenta*
P20_2/PN_F2	"	"	"
P20_3/PN_F3	"	"	"
P20_4/PN_F4	"	"	"
P20_5/PN_F5	"	"	"
P20_6/PN_F6	"	"	"
P20_7/PN_F7	"	"	"
P20_8/PN_F8	"	"	"
P20_9/PN_F9	"	"	"
P20_10/PN_F10	"	"	"
P20_11/PN_F11	"	"	"
P20_12/PN_F12	"	"	"

each strain and on different dates to check culture stability and repeatability of the results.

Measurements

Particle concentrations and cell shape (elongation and length) and their physiology (number of cell per chain, complexity, etc.) were characterized by pulse shape-based flow-cytometry (Cytosense, CS-2015-77). The large tube diameter (800 μm) of this flow cytometer permitted a reliable count of particles up to 250 μm without breaking any cells in the chain. Measurements were taken with two different settings. The first one had a duration of 10 min and a low sampling flow (5 μL · s^{-1}), permitting some image acquisition for the detected events (analyzed volume of 3 mL). The second analysis was carried out with a higher flow rate (10 μL · s^{-1}) but without image acquisition, to increase the number of detected events and the accuracy of the density estimates (analyzed volume of 6 mL). Sub-populations were easily defined with a manual gating (Figure 1). Then, the cell densities were diluted for the following experiments in order to use similar densities (10^6 particles · (L^{-1}) in all experiments.

The protocol detailed in Font-Muñoz et al. (2021) was used to estimate the particle size distribution and their orientations according to the mixing conditions. Briefly, experiments were carried out in a small volume (~100 mL) flow-through chamber from a LISST-100X (Sequoia Scientific). This configuration made it possible to take simultaneous measurements of cell orientation and transmission after a mixing period (100 s), creating randomly oriented cells as an initial condition. To study the effect of light conditions on cell orientations, the light and dark periods were alternated. The cells were first illuminated with white light (10 μmol photons · m^{-2} · s^{-1}) for 50 min, followed by 45 min of complete darkness and a 1-h light period.

To supplement the cell orientation measurements, video-microscopy 2D observations of the sinking cells were also performed (Figure S1 in the Supporting Information). To suppress convective currents, a salinity-stabilized water column was produced in a flask (250 mL) following the method described by O'Brien et al. (2006). According to the initial and final salinities used (30 and 32, respectively), the vertical gradient was 0.66 · cm^{-1}. A laser sheet (width of 400 μm, Laser Newport, 402 nm powered at 30 mA) was created in the flask, and images were acquired with a CMOS sensor (resolution 1×10^6 pixels) and a telecentric lens (4X). The sensitivity gain was set at 100. A frame rate of 2 images · s^{-1} was used, and the image resolution was set to 1.825 pixels · μm^{-1}. The observed volume was 1.3 μL. To avoid a residual convection created by laser illumination and a lethal impact on the cells, a shutter synchronized with the camera was also used to reduce the exposure time. The time lag between creation of the gradient and recording of the image was close to 5 min. The quality of the density gradient was checked during the post-processing of the video sequences by the absence of horizontal displacement. A threshold of 2 μm · s^{-1} was used to remove bias sequences.

Data processing

Laser in-situ scattering and transmissometry (LISST) measurements (abundances of 32 size classes ranging from 2.73 to 250 μm) were processed as detailed

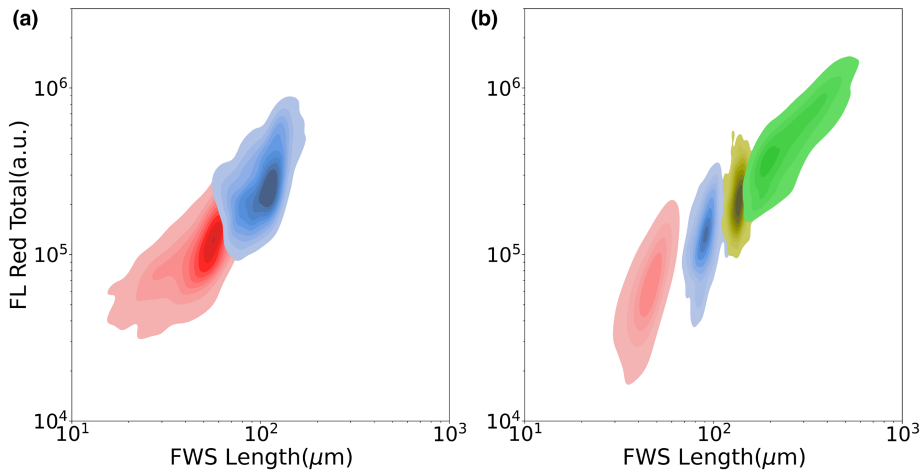

FIGURE 1 Clusters of chain lengths (number of cells per length) for *Pseudo-nitzschia fraudulenta* and *P. pungens* (a and b, respectively) according to the length of the forward scatter pulse shape signal and the total red fluorescence for the event (FWS and FL Red, respectively). The number of cells per cluster ranged from 1 to 4 (C1, C2, C3, and C4+, respectively, with the longest chains having the highest fluorescence). Cluster densities were estimated by subsampling all flow cytometric measurements to obtain the same number of events per cluster. For *P. fraudulenta*, the maximum significance length was only two cells per chain in our cultures whereas for *P. pungens*, the C4+ cluster includes chains with at least four cells.

in Font-Muñoz et al. (2020, 2021). Measurements of nearly elongated particles were r and k interpreted in terms of the relative variation of two size bands (r_1 and r_2 extracted from the LISST size classes) associated to the major and minor cell axis length. The size bands were identified by *K*-means clustering because several close size classes can have the same temporal variations. In addition, due to the 2D projection of LISST measurements, the ratio between the signal from each of these two size bands is a scalar proxy for the mean cell orientation. A temporal variation of the mean cell orientation will lead to an anticorrelation between the signal for each size bands (the major axis being more or less visible according to the 2D projection). A wavelet analysis was then used on this ratio to extract its temporal variability. As explained in a previous work (Font-Muñoz et al., 2021), a significant temporal variability of ratio involved a consistent evolution of the orientation of the bulk of the suspended particles.

Recorded videos obtained by video-microscopy were analyzed using two Python libraries: Scikit-image (0.18.1, van der Walt et al., 2014) and Trackpy (0.4.2, Crocker & Grier, 1996). Images were segmented to extract one object per particle using a Sobel operator (Kroon, 2009) and a watershed algorithm (Neubert & Protzel, 2014). The properties of the object (size, gray levels, etc.) were then used to clear incorrect detections (particles smaller than the expected cell size, etc.) associated with detrital particles, particles out of the field of view, or weakly illuminated particles. To calculate the trajectories for each particle, a simple algorithm (assuming a Brownian diffusion between frames) was used with two parameters: The highest displacement allowed between two frames (*d*) and the number of frames (*n*) for which a particle can be undetected. According to the image frame rate and the observed sinking rates, *d* and *n* were fixed to 27 μm·s^{-1} and two images, respectively.

RESULTS

Culture and the chain length

Flow cytometry data revealed specific and stable structures of the cultivated populations during the experiment (Figure 2). *Pseudo-nitzschia fraudulenta* cultures were dominated by individual cells (>97% of the particles in cluster 1C). The average length of all particles could be estimated with the pulse shape length of the forward scatter (FWS) signal, but the analysis of flow cytometry (FCM) images with individual cells provided more accurate measurements (Figure 3). Their length and width in our cultures were estimated to 39 and 8 μm, respectively. Conversely, *P. pungens* cultures were characterized by a broad diversity in terms of chain length (from 1 to more than 5 connected cells), with a maximum chain length longer than 0.5 mm and an average length of 150 μm. The largest fraction of cells was included in the cluster of 4 cells (4C+ cluster). Individual cells (1C cluster) constituted less than 50% of the suspended particles and a limited fraction of the cells. Given that

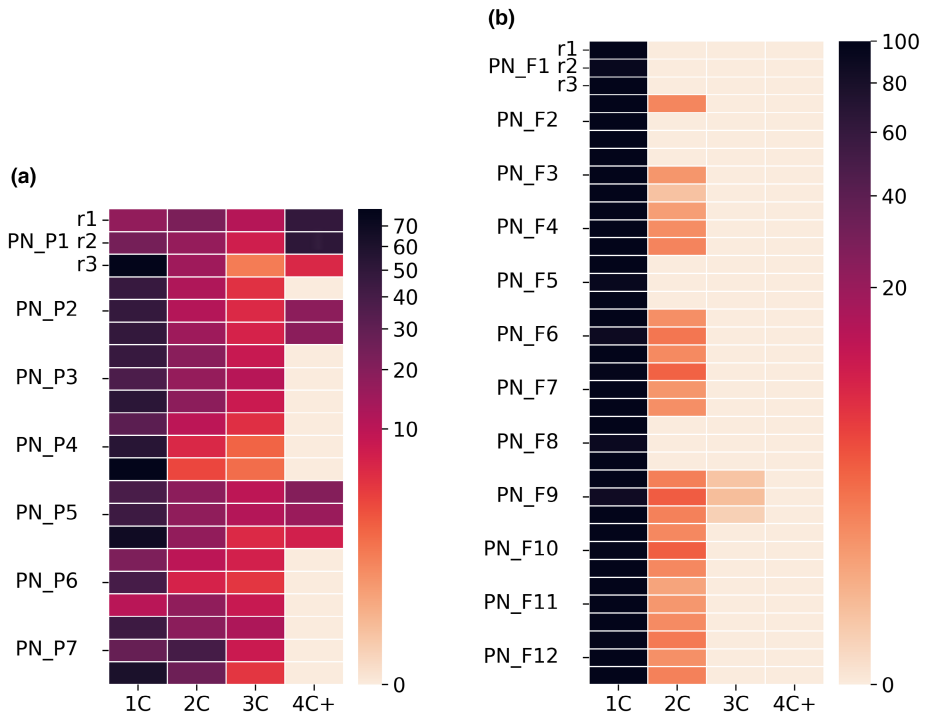

FIGURE 2 Relative abundances of chain length for all strains and replicates (r1 to r3) of P. punges and P. fraudulenta cultures (a and b respectively). Clusters were made for chain lengths ranging from 1 to 3 cells per chain (C1 to C3). The 4C+ cluster included all chains with four cells and more.

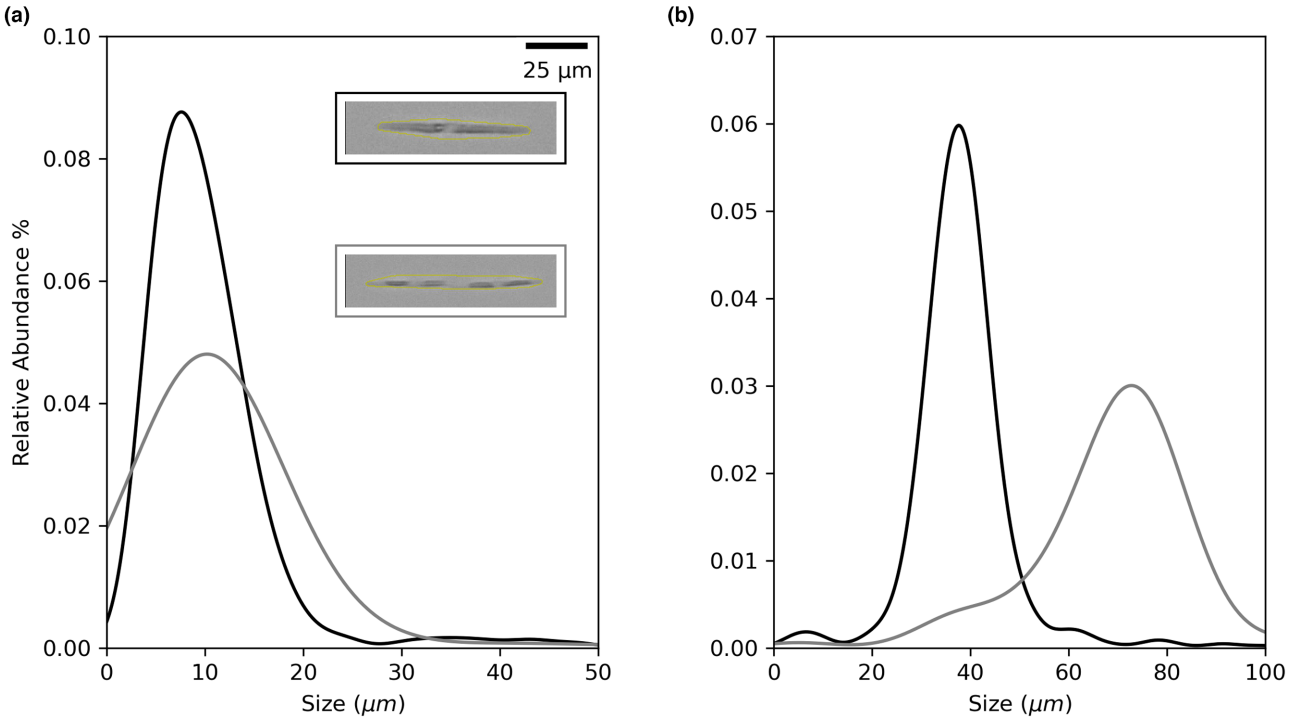

FIGURE 3 Distributions of minor (a) and major (b) axis values for the PN-F2 clusters with either one or two cells (black and gray, respectively). The parameters were directly extracted from the FCM images (minor axis), and the forward scatter pulse shape signal (major axis). For illustration, one image sample for each cluster was included with a scale bar.

the particle length of these *P. pungens* strains was longer than the LISST size range (with a maximum measurable length for a particle of 250 µm), several attempts were made to remove the long chains using prefiltration. However, since the width of the chains was the same as for individual cells, it made filtration useless and precluded their orientation analysis with the LISST method. Furthermore, laser diffractometry only provided information on the orientation dynamics of a suspension of similar non-spherical particles (e.g., individual cells or chains of the same length; Font-Muñoz et al., 2020). Unfortunately, only the LISST experiments with the *P. fraudulenta* strains could be analyzed using this method.

Orientation of sinking particles

The *K*-means analysis identified size classes for *Pseudo-nitzschia fraudulenta* minor and major axes measuring 6 and 30 µm, respectively (Figure S2 in the Supporting Information). These measurements were fully consistent with size estimates obtained through optical microscopy and flowcytometry. Similar to the observations for *P. delicatissima* (Font-Muñoz et al., 2021), a few minutes after the end of the initial mixing and a period of random orientation, cells were mainly reoriented in a vertical position. The orientation of *P. fraudulenta* displayed a clear difference associated with the light/dark phases (Figure 4). Some synchronic oscillations were observed only during the light phases and were characterized by a periodic variation with a period between 50 and 100 s. These oscillations were linked to a periodic variation of the average cell orientation around their equilibrium position. The existence of such oscillations implies a synchronization process that is described and discussed in a previous work (Font-Muñoz et al., 2021). It is worth noting that the oscillations appeared and disappeared quickly (in less than 1 min) after alternations of the light conditions. During the dark phases, oscillations were almost always non-significant (Figure 5) compared with those under illuminated conditions, despite a great variability in their associated powers. The oscillation frequencies were also surprisingly similar (close to 100 s) between the strains and species (*P. delicatissima* and *P. fraudulenta*).

Sinking rates

Unlike the method using the LISST, measurements of sinking rates by video-microscopy—being not limited by the particle length, orientation, and sinking rate of all cells and chains—were analyzed for both species. The horizontal advection observed in the flask was one order of magnitude lower than the vertical sinking rates (Figure S3 in the Supporting Information). *Pseudo-nitzschia pungens* chains were mainly oriented horizontally ($\alpha = 0$) during their sedimentation (Figure 6a)

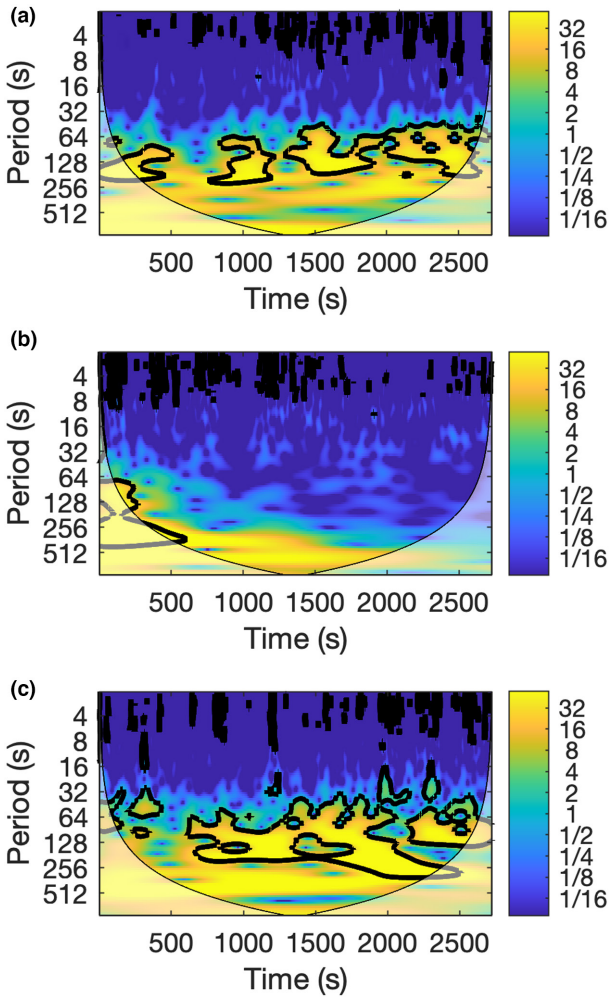

FIGURE 4 Wavelet analysis of the dimensionless axis ratio over time during the light (a, c) and dark (b) periods for strain PN_F4. The power is indicated by the color bar, ranging from low to high power). The threshold above the 95% confidence interval of a red-noise spectrum is indicated with a thick black line. Lighter shades show the cone of influence where the edge effects may distort the Fourier analysis.

whereas *P. fraudulenta* cells appeared to be more randomly distributed, with less visible vertical orientation than was observed with the LISST (Figure 6b). Due to the size of individual cell versus chains, their major axes and their orientations were less well defined. Observations of recorded sequences demonstrated that cell chains were mainly oriented horizontally with a u-shape (Figures S4 in the Supporting Information). By selecting particles of *P. pungens* with a size smaller than 360 μm (less than 4 cells) on the video-microscopic image, in order to increase the proportion of individual cells, their orientation converged toward the observed orientation for *P. fraudulenta* cells. This size threshold appeared very large compared to the real cell size, but the diffraction associated with the fluorescence process strongly increased the particle size.

Similarly, sinking rates were significantly different between the two species. The average sinking rates for *Pseudo-nitzschia pungens* and *P. fraudulenta* were estimated to be 3.22 and 1.82 $\mu m \cdot s^{-1}$, respectively. Small particles in *P. pungens* cultures had a lower sinking rate (2.1 $\mu m \cdot s^{-1}$) than the observed average value, but their rate remained significantly higher than the one observed for individual *P. fraudulenta* cells.

DISCUSSION

Due to the impact of where and how cells are positioned in the water column on the growth of *Pseudo-nitzschia pungens* and *P. fraudulenta*, this study was conducted to estimate intra- and inter-specific variability of cell orientation and cell sinking rates. We clearly demonstrated that the communication process, leading to consistent oscillation of individual cells around a vertical orientation at equilibrium, was widespread among pennate diatoms and produced similar frequencies. However, sinking rates appeared primarily driven by whether or not chains were produced. As a consequence, sinking rates appear to be highly specific. This result leads us to conclude that each *Pseudo-nitzchia* species can be characterized by a specific clearance rate in the surface layer after a bloom event as well as by a specific contribution to marine snow formation (Arguedas-Leiva et al., 2022). Our results also shown that sedimentation of *Pseudo-nitzschia* chains was governed by the same dynamics as flexible fibers and that theoretical results could be applied.

Before explaining the processes leading to cell orientation, we must say that with all the strains of the two selected species and our culture conditions, this experiment fell within the general framework of previous studies conducted at microscale. Given the cell densities, observed sinking rates, and chain lengths, the sedimentation of *Pseudo-Nitzchia* was characterized by low Reynolds numbers (*Re* between 2×10^{-2} and 3×10^{-5} for 500 μm cell chains to individual cells, respectively) in diluted conditions (Botte et al., 2013, $n(l/2)^3<1$; from 3.3×10^{-6} to 0.4×10^{-3} for particle lengths ranging from 30 to 150 μm). Consistent with theoretical models, solitary cells predominantly settled vertically owing to their oblong cell shape, while chains (at least for *P. pungens*) tended to settle horizontally.

The reorientation process for chains into horizontal positions was, however, not straightforward because chain elongation was insufficient by itself. In the case of *Pseudo-Nitzchia pungens* strains, this reorientation was largely influenced by the degree of the flexibility of junctions between cells (Nguyen & Fauci, 2014). Higher flexibility allowed the sedimentation dynamics of the chains to mimic the sedimentation dynamics of a flexible fiber (du Roure et al., 2019). As described in previous studies, at low Reynolds numbers (<0.01), a long, uniform particle, such as a fiber, dynamically

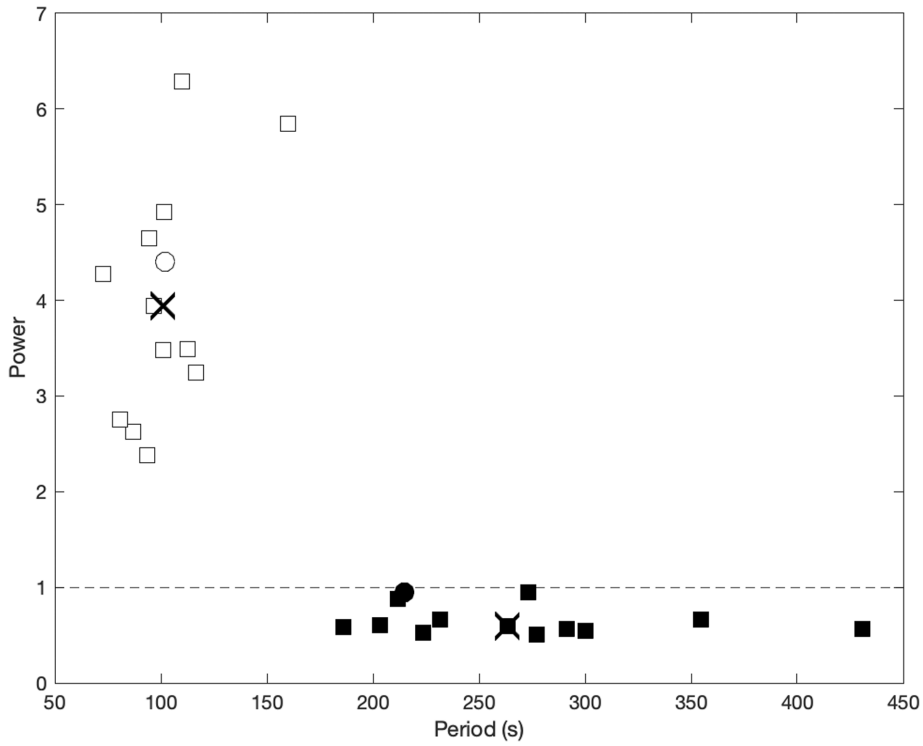

FIGURE 5 Power spectrum (dimensionless) and oscillation periods provided by the wavelet analysis for the different strains of *Pseudo-nitzschia fraudulenta* (square symbols) during the dark and light periods (filled and open symbols, respectively). Data located *in* the edge influence were removed. The results obtained with one *P. delicatissima* strain (Font-Muñoz et al., 2021) are indicated as a reference (circle symbols), and the average value is given for *P. fraudulenta* (X symbol). The dotted line indicates the significant detection level for the oscillations.

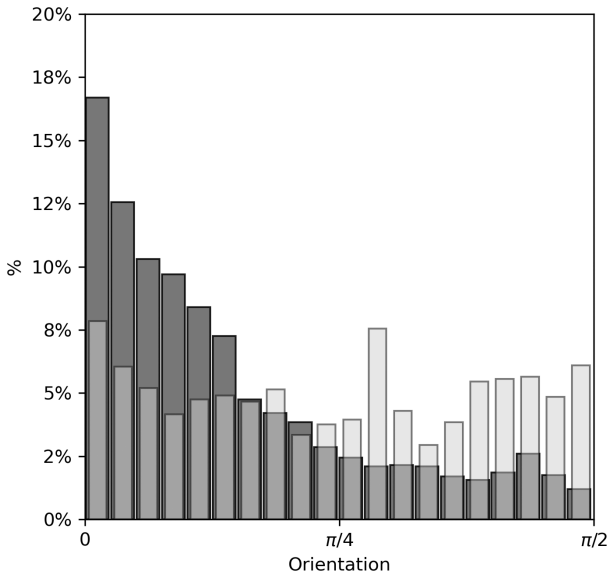

FIGURE 6 Cell orientation estimated by video-microscopy for *Pseudo-nitzschia pungens* and *Pseudo-nitzschia fraudulenta* (gray and light gray, respectively). Values range from 0 to $\pi/2$ for the horizontal and vertical orientations, respectively.

deforms in response to the viscous stresses acting on it. The flexible fiber undergoes a torque that orients it toward a horizontal position (i.e., with its longitudinal axis perpendicular to the direction of gravity regardless of its initial configuration) and adopts a "U" shaped position (Li et al., 2013; Marchetti et al., 2018). This "U" shape is precisely what we observed for the diatom chains in our experiments (see Figure S4). Therefore, this work provides rare experimental evidence that the sedimentation of *Pseudo-nitzschia* chains is governed by the same dynamics as flexible fibers.

By accepting the flexible fiber model, some theoretical properties can be used, such as how the fiber shape at equilibrium depends on the relative magnitude of the gravitational force and the elastic restoring force. Due to the observed shape of our chains (a "U" shape with a relatively wide opening at the top of the U), a small ratio between these forces can be assumed. Consequently, the theoretical steady velocity should be close to the settling velocity of a rigid chain horizontally oriented (du Roure et al., 2019) and significantly below the settling velocity expected for such a vertically oriented chain. *Pseudo-nitzschia pungens* cells, therefore, significantly decrease their sinking rates. This process could be very common in natural environment due to the high local shear variability (in space and time) in coastal waters, and similar orientations have already been observed in the marine environment under weak shear conditions (Nayak et al., 2018; Talapatra et al., 2013).

Our results also demonstrate that it is challenging to link the modulation of the chain length to one specific factor. For example, assumptions about the evolutionary advantages of long chains solely for light harvesting during periods of low mixing may be too simplistic. Although it has been suggested that a horizontal orientation could improve light harvesting by up to 24% compared to a random orientation (McFarland et al., 2020), our observations indicate that the actual benefits would be nuanced. First, without considering buoyancy regulation the sinking rate of the chains remains positively correlated with their length at the interspecific level. Their increase would thereby decrease the light resource by deepening their average distribution. Second, because individual cells were observed to be regularly tilted around the vertical orientation, they significantly reduced the expected light limitation (Font-Muñoz et al., 2021).

In addition, modification of the chain length was strongly related to the cell growth rate (some cellular divisions are required for the increase in length). Therefore, the formation of chains or their elongation as a specific response to an environmental pressure may only occur at the daily scale, and a fast response (at least for the length increase) to external factors is unlikely. The modulation of chain length in the environment is complex and related to the large set of factors encountered by the cells over the preceding few days Bjærke et al. 2015.

Finally, although existing knowledge had already established the influence of cell orientation on sinking rates, movement trajectories, and cell concentrations (Botte et al., 2013; Font-Muñoz et al., 2019; Metzger et al., 2005), our results reveal that the communication process leading to consistent oscillations is widespread among pennate diatoms and occurs with frequencies that are surprisingly close to those observed with *Pseudo-nitzschia delicatessima* (Font-Muñoz et al., 2021). Assuming the conservation of a biological trait across phylogeny should underline its relevance, this biological response seems to be of primary interest. Although we have yet to describe the ecological consequences of such a process and unravel the cellular process involved in such a fast response, our observations highlight that the perception capacities of cells are more developed than expected. It is conceivable that many of the previously described communication processes (photoreceptors, chemical exudation, calcium signaling, etc.) collectively set a sophisticated sensor network to perceive the surrounding environment and to permit acclimation processes at different time scales. The fast change in expression due to the turbulence observed by Amato et al. (2017) pushes this theory in that direction, and cells seem to be more and more distant from passive particles.

AUTHOR CONTRIBUTIONS

M. Sourisseau: Conceptualization (equal); data curation (equal); formal analysis (equal); funding acquisition (lead); investigation (equal); methodology (equal); project administration (lead); supervision (equal); validation (equal); visualization (equal); writing – original draft (lead); writing – review and editing (equal). **J. Font-Muñoz:** Conceptualization (equal); data curation (equal); formal analysis (equal); investigation (equal); methodology (equal); project administration (equal); supervision (equal); validation (equal); visualization (equal); writing – original draft (equal); writing – review and editing (equal). **S. Bellouche:** Data curation (equal); formal analysis (equal); validation (equal); visualization (equal). **O. Fauvarque:** Methodology (supporting); validation (supporting); writing – review and editing (supporting). **J. Rouxel:** Methodology (supporting); validation (supporting); writing – review and editing (supporting). **M. Tardivel:** Methodology (supporting); validation (supporting); writing – review and editing (supporting). **A. Sauvey:** Resources (supporting).

ACKNOWLEDGMENTS

We thank J. Quere for its support with regards to the molecular analysis.

FUNDING INFORMATION

This research was supported by the ISblue project, Intersdisciplinary graduate school for the Blue Planet (ANR-17-EURE-0015), and co-funded by a grant from the French government under the "Investissements d'Avenir" program and a grant from the Regional Council of Brittany (SAD program). J.S Font-Muñoz is grateful for the funding received through an individual postdoctoral fellowship 'Margalida Comas' (PD/018/2020) from Govern de les Illes Balears and Fondo Social Europeo.

ORCID

M. Sourisseau https://orcid.org/0000-0002-0778-0076

REFERENCES

Amato, A., Dell'Aquila, G., Musacchia, F., Annunziata, R., Ugarte, A., Maillet, N., Carbone, A., Ribera d'Alcalà, M., Sanges, R., Iudicone, D., & Ferrante, M. I. (2017). Marine diatoms change their gene expression profile when exposed to microscale turbulence under nutrient replete conditions. *Scientific Reports*, *7*, 3826. https://doi.org/10.1038/s41598-017-03741-6

Anderson, L. W. J., & Sweeney, B. M. (1978). Role of inorganic ions in controlling sedimentation rate of a marine centric diatom ditylum brightwelli 1,2. *Journal of Phycology*, *14*, 204–214. https://doi.org/10.1111/j.1529-8817.1978.tb02450.x

Arguedas-Leiva, J.-A., Słomka, J., Lalescu, C. C., Stocker, R., & Wilczek, M. (2022). Elongation enhances encounter rates between phytoplankton in turbulence. *Proceedings of the National Academy of Sciences*, *119*(32), e2203191119. https://doi.org/10.1073/pnas.2203191119

Bjærke, O., Jonsson, P. R., Alam, A., & Selander, E. (2015). Is chain length in phytoplankton regulated to evade predation? *Journal*

of Plankton Research, *37*(6), 1110–1119. https://doi.org/10.1093/plankt/fbv076

Botte, V., Ribera D'Alcalà, M., & Montresor, M. (2013). Hydrodynamic interactions at low Reynolds number: An overlooked mechanism favouring diatom encounters. *Journal of Plankton Research*, *35*(4), 914–918. https://doi.org/10.1093/plankt/fbt033

Brandenburg, K. M., Wohlrab, S., John, U., Kremp, A., Jerney, J., Krock, B., & Van de Waal, D. B. (2018). Intraspecific trait variation and trade-offs within and across populations of a toxic dinoflagellate. *Ecology Letters*, *21*(10), 1561–1571. https://doi.org/10.1111/ele.13138

Carter, G. S., Gregg, M. C., & Lien, R.-C. (2005). Internal waves, solitary-like waves, and mixing on the monterey bay shelf. *Continental Shelf Research*, *25*, 1499–1520. https://doi.org/10.1016/j.csr.2005.04.011

Crocker, J. C., & Grier, D. G. (1996). Methods of digital video microscopy for colloidal studies. *Journal of Colloid and Interface Science*, *179*(1), 298–310. https://doi.org/10.1006/jcis.1996.0217

Eppley, R. W., Holmes, R. W., & Strickland, J. D. H. (1967). Sinking rates of marine phytoplankton measured with a fluorometer. *Journal of Experimental Marine Biology and Ecology*, *1*(2), 191–208. https://doi.org/10.1016/0022-0981(67)90014-7

Font-Muñoz, J. S., Jeanneret, R., Arrieta, J., Anglès, S., Jordi, A., Tuval, I., & Basterretxea, G. (2019). Collective sinking promotes selective cell pairing in planktonic pennate diatoms. *Proceedings of the National Academy of Sciences*, *116*(32), 15997–16002. https://doi.org/10.1073/pnas.1904837116

Font-Muñoz, J. S., Jeanneret, R., Tuval, I., & Basterretxea, G. (2020). Method for the determination of preferential orientation of marine particles from laser diffraction measurements. *Optics Express*, *28*(9), 14085–14099. https://doi.org/10.1364/OE.390388

Font-Muñoz, J. S., Sourisseau, M., Cohen-Sánchez, A., Tuval, I., & Basterretxea, G. (2021). Pelagic diatoms communicate through synchronized beacon natural fluorescence signaling. *Science Advances*, *7*(51), eabj5230. https://doi.org/10.1126/sciadv.abj5230

Gemmell, B. J., Oh, G., Buskey, E. J., & Villareal, T. A. (2016). Dynamic sinking behaviour in marine phytoplankton: Rapid changes in buoyancy may aid in nutrient uptake. *Proceedings of the Royal Society B: Biological Sciences*, *283*(1840), 20161126. https://doi.org/10.1098/rspb.2016.1126

Gross, F., Zeuthen, E., & Yonge, M. (1997). The buoyancy of plankton diatoms: A problem of cell physiology. *Proceedings of the Royal Society of London, Series B: Biological Sciences*, *135*(880), 382–389. https://doi.org/10.1098/rspb.1948.0017

Karp-Boss, L., Boss, E., & Jumars, P. A. (1996). Nutrient fluxes to planktonic osmotrophs in the presence of fluid motion. *Oceanography and Marine Biology: An Annual Review*, *34*, 71–107.

Kroon, D. (2009). *Numerical optimization of kernel based image derivatives*; Short Paper; University of Twente: Enschede, The Netherlands 2009; Volume 3.

Kruk, C., Huszar, V. L. M., Peeters, E. T. H. M., Bonilla, S., Costa, L., Lürling, M., Reynolds, C. S., & Scheffer, M. (2010). A morphological classification capturing functional variation in phytoplankton. *Freshwater Biology*, *55*(3), 614–627. https://doi.org/10.1111/j.1365-2427.2009.02298.x

Kruk, C., & Segura, A. M. (2012). The habitat template of phytoplankton morphology-based functional groups. *Hydrobiologia*, *698*(1), 191–202. https://doi.org/10.1007/s10750-012-1072-6

Li, L., Manikantan, H., Saintillan, D., & Spagnolie, S. E. (2013). The sedimentation of flexible filaments. *Journal of Fluid Mechanics*, *735*, 705–736. https://doi.org/10.1017/jfm.2013.512

Marchetti, B., Raspa, V., Lindner, A., du Roure, O., Bergougnoux, L., Guazzelli, É., & Duprat, C. (2018). Deformation of a flexible fiber settling in a quiescent viscous fluid. *Physical Review Fluids*, *3*(10), 104102. https://doi.org/10.1103/PhysRevFluids.3.104102

Margalef, R. (1978). Life-forms of phytoplankton as survival alternatives in an unstable environment. *Oceanologica Acta*, *1*(4), 493–509.

May, C. L., Koseff, J. R., Lucas, L. V., Cloern, J. E., & Schoellhamer, D. H. (2003). Effects of spatial and temporal variability of turbidity on phytoplankton blooms. *Marine Ecology Progess Series*, *254*, 111–128. https://doi.org/10.3354/meps254111

McFarland, M., Nayak, A. R., Stockley, N., Twardowski, M., & Sullivan, J. (2020). Enhanced light absorption by horizontally oriented diatom colonies. *Frontiers in Marine Science*, *7*, 494. https://doi.org/10.3389/fmars.2020.00494

Metzger, B., Guazzelli, É., & Butler, J. E. (2005). Large-scale streamers in the sedimentation of a dilute fiber suspension. *Physical Review Letters*, *95*(16), 164506. https://doi.org/10.1103/PhysRevLett.95.164506

Naselli-Flores, L., Padisák, J., & Albay, M. (2007). Shape and size in phytoplankton ecology: Do they matter? *Hydrobiologia*, *578*(1), 157–161. https://doi.org/10.1007/s10750-006-2815-z

Nayak, A. R., McFarland, M. N., Sullivan, J. M., & Twardowski, M. S. (2018). Evidence for ubiquitous preferential particle orientation in representative oceanic shear flows. *Limnology and Oceanography*, *63*(1), 122–143. https://doi.org/10.1002/lno.10618

Neubert, P., & Protzel, P. (2014). Compact watershed and preemptive SLIC: On improving trade-offs of superpixel segmentation algorithms. In *2014 22nd international conference on pattern recognition*, Stockholm, Sweden, pp. 996–1001. https://doi.org/10.1109/ICPR.2014.181

Nguyen, H., & Fauci, L. (2014). Hydrodynamics of diatom chains and semiflexible fibres. *Journal of the Royal Society Interface*, *11*(96), 20140314. https://doi.org/10.1098/rsif.2014.0314

Noyer, C., Abot, A., Trouilh, L., Anton Leberre, V., & Dreanno, C. (2015). Phytochip: Development of a DNA-microarray for rapid and accurate identification of *Pseudo-nitzschia* spp and other harmful algal species. *Journal of Microbiological Methods*, *112*, 55–66. https://doi.org/10.1016/j.mimet.2015.03.002

O'Brien, K. R., Waite, A. M., Alexander, B. L., Perry, K. A., & Neumann, L. E. (2006). Particle tracking in a salinity gradient: A method for measuring sinking rate of individual phytoplankton in the laboratory. *Limnology and Oceanography: Methods*, *4*(9), 329–335. https://doi.org/10.4319/lom.2006.4.329

Padisák, J., Soróczki-Pintér, É., & Rezner, Z. (2003). Sinking properties of some phytoplankton shapes and the relation of form resistance to morphological diversity of plankton – An experimental study. *Hydrobiologia*, *500*(1), 243–257. https://doi.org/10.1023/A:1024613001147

Raven, J. A., & Beardall, J. (2022). Evolution of phytoplankton in relation to their physiological traits. *Journal of Marine Science and Engineering*, *10*, 194. https://doi.org/10.3390/jmse10020194

du Roure, O., Lindner, A., Nazockdast, E. N., & Shelley, M. J. (2019). Dynamics of flexible fibers in viscous flows and fluids. *Annual Review of Fluid Mechanics*, *51*(1), 539–572. https://doi.org/10.1146/annurev-fluid-122316-045153

Słomka, J., & Stocker, R. (2020). On the collision of rods in a quiescent fluid. *Proceedings of the National Academy of Sciences*, *117*(7), 3372–3374. https://doi.org/10.1073/pnas.1917163117

Talapatra, S., Hong, J., McFarland, M., Nayak, A. R., Zhang, C., Katz, J., Sullivan, J., Twardowski, M., Rines, J., & Donaghay, P. (2013). Characterization of biophysical interactions in the water column using in situ digital holography. *Marine Ecology Progress Series*, *473*, 29–51. https://doi.org/10.3354/meps10049

Visser, A. W., & Jonsson, P. R. (2000). On the reorientation of non-spherical prey particles in a feeding current. *Journal of Plankton Research*, *22*(4), 761–777. https://doi.org/10.1093/plankt/22.4.761

Walsby, A. E. (1978). The properties and buoyancy-providing role of gas vacuoles in *Trichodesmium* Ehrenberg. *British Phycological Journal*, *13*(2), 103–116. https://doi.org/10.1080/00071617800650121

Walsby, A. E., & Holland, D. P. (2006). Sinking velocities of phytoplankton measured on a stable density gradient by laser scanning. *Journal of the Royal Society Interface*, *3*(8), 429–439. https://doi.org/10.1098/rsif.2005.0106

van der Walt, S., Schönberger, J. L., Nunez-Iglesias, J., Boulogne, F., Warner, J. D., Yager, N., Gouillart, E., & Yu, T. (2014). scikit-image: Image processing in Python. *PeerJ*, *2*, e453. https://doi.org/10.7717/peerj.453

Weithoff, G. (2003). The concepts of 'plant functional types' and 'functional diversity' in lake phytoplankton – A new understanding of phytoplankton ecology? *Freshwater Biology*, *48*(9), 1669–1675. https://doi.org/10.1046/j.1365-2427.2003.01116.x

Wirtz, K., & Smith, S. L. (2020). Vertical migration by bulk phytoplankton sustains biodiversity and nutrient input to the surface ocean. *Scientific Reports*, *10*(1), 1142. https://doi.org/10.1038/s41598-020-57890-2

Zehr, J. P., Weitz, J. S., & Joint, I. (2017). How microbes survive in the open ocean. *Science*, *357*(6352), 646–647. https://doi.org/10.1126/science.aan5764

SUPPORTING INFORMATION

Additional supporting information can be found online in the Supporting Information section at the end of this article.

Figure S1-S4

How to cite this article: Sourisseau, M., Font-Muñoz, J., Bellouche, S., Fauvarque, O., Rouxel, J., Tardivel, M., & Sauvey, A. (2024). Sinking rates, orientation, and behavior of pennate diatoms. *Journal of Phycology*, *00*, 1–10. https://doi.org/10.1111/jpy.13463